Short and Medium Range Order in Sodium Aluminoborate Glasses. 2. Site Connectivities and Cation Distributions Studied by Rotational Echo Double Resonance NMR Spectroscopy

Marko Bertmer, Lars Züchner, Jerry C. C. Chan, and Hellmut Eckert*

Institut für Physikalische Chemie, Westfälische Wilhelms-Universität Münster, Schlossplatz 7, D-48149 Münster, Germany

Received: November 29, 1999; In Final Form: March 3, 2000

A quantitative NMR strategy is developed for the study of the network connectivity (intermediate range structure) and the cation distribution in the sodium aluminoborate glass system. The strategy is based on the analysis of rotational echo double resonance (REDOR) spectroscopy applied to the glasses and the crystalline model compounds $Li_6Al_2(BO_3)_4$, $NaBO_2$, and $Na_2B_4O_7$. The heterodipolar multispin interaction between the quadrupolar spin systems $^{27}Al \leftrightarrow {}^{11}B$ and $^{23}Na \leftrightarrow {}^{11}B$ is analyzed in terms of approximate second moments, which are extracted from REDOR data measured at short dipolar evolution times. On the basis of $^{27}Al\{^{11}B\}$ and $^{11}B\{^{27}Al\}$-REDOR results, the framework connectivity distribution is extracted and compared to statistical and preferential bonding distribution scenarios, respectively. The sodium aluminoborate system is characterized by a large degree of bonding regularity in the framework. Four-coordinated aluminum is preferentially linked to $BO_{3/2}$ and $BO_{2/2}O^-$ units and vice versa, while linking between two four-coordinate units is disfavored, as expected on the basis of bond valence considerations. In glasses with low aluminum contents and/or high sodium contents, there is a greater tendency toward a randomization of connectivities. Spatial correlations between the sodium nuclei and the boron atoms in the network are probed by complementary $^{23}Na\{^{11}B\}$- and $^{11}B\{^{23}Na\}$-REDOR experiments. The results reveal that both the three- and the four-coordinated boron species interact equally strongly with sodium cations, consistent with an overall homogeneous cation distribution.

Introduction

Interest in noncrystalline solids and glasses as a subject of basic and applied science has increased dramatically in recent years. Detailed structural information is sought in order to provide a rationale for the compositional control of physical properties. Owing to the lack of long-range periodicity the structural problem in glasses can be discussed on different length scales: short-range bonding (1.5−3.0 Å), medium range structure (3.0−10 Å), and nanostructure (10−100 Å). High-resolution solid-state NMR spectroscopy has been particularly instrumental in addressing questions of short-range bonding, providing identification and quantification of distinct coordination polyhedra in the network.[1−3] To date, many oxide glass systems are quite well-understood in these terms. However, the mode in which local environments are linked to constitute medium range structure in such systems has remained one of the great challenges in glass science.[4] In the present study we will introduce a novel, generally applicable solid state NMR strategy to address this question. Specifically, we will apply this strategy to sodium aluminoborate glasses, whose frameworks are constructed from four principal building blocks: tetrahedral $BO_{4/2}^-$ and AlO_4^- units, trigonal $BO_{3/2}$ groups bound to all bridging oxygen, and $BO_{2/2}O^-$ sites containing one nonbridging oxygen atom.[5−9] In addition, small amounts of five- and six-coordinated aluminum sites are present.[8] In part I of this study we have deduced the quantitative populations of these sites from a detailed analysis of the ^{27}Al and ^{11}B magic-angle-spinning spectra.[8] Here, in part II of this study, we will address the issue of medium range structure. Must the network be considered as an extended continuum or are certain glass constituents spatially segregated? Are the building blocks linked in a statistical manner or is there evidence for preferred connectivities and/or spatial correlations? What is the spatial relationship between the sodium cation and the network former species in these glasses? Concerning site connectivities, Bunker, Kirkpatrick and Brow have already made specific predictions based on the bond valence concept.[9,10] For each of the framework atoms a bond valence is defined by BV = (formal oxidation number)/(coordination number).

TABLE 1: Bond Valences BV for the Central Atoms in Various Typical Framework Sites in Glasses

framework site	BV
$BO_{3/2}$	1.0
$BO_{4/2}^-$	0.75
$AlO_{4/2}^-$	0.75
Al(V)	0.6
Al(VI)	0.5
$SiO_{4/2}$	1.0
$O{=}PO_{3/2}$	1.25

Table 1 lists values for typical framework sites in glasses. In most cases, two framework sites are linked by a bridging oxygen atom; however, three- and four-coordinate oxygen species are also known to exist. The stability of a particular oxygen configuration depends on how effectively its negative formal charge (−2) is compensated by the positively charged ligands. To this end one calculates the excess local charge according to

$$C = \sum_i BV_i - 2$$

$C = 0$ corresponds to perfect charge compensation and

* To whom correspondence should be addressed.

10.1021/jp9941918 CCC: $19.00
Published on Web 06/24/2000

maximum stability of a bridging oxygen atom. If $C > 0$, the oxygen atom is destabilized (overbonded). If $C < 0$ (underbonded oxygen), additional charge compensation is possible by interaction with positively charged network modifier cations. Application of these ideas to aluminoborate glasses has resulted in the following principal predictions:[10] (1) the formation of AlO_5 and AlO_6 polyhedra requires the presence of three- or four-coordinate oxygen, (2) direct links between negatively charged units such as $BO^-_{4/2}$ or/and AlO_4^- are less stable than $BO_{3/2}-AlO^-_{4/2}$ links, and (3) the local coordination environments and site connectivities are also influenced by the ionic potentials of the network modifier cations.

It would be of great interest to put the above predictions to a direct experimental test. Thus, the structural focus of the present contribution concerns the site connectivities among the various boron and aluminum units present in these glasses. While chemical shift spectroscopy, combined with a good deal of interpretation, has provided certain inferences in this regard,[8] more quantitative evidence is required. New high-resolution solid state double resonance NMR experiments have offered great promise for this purpose. In particular, the rotational echo double resonance (REDOR) NMR method has proven quite useful for measuring the strength of internuclear dipole−dipole interactions.[11,12] Since these interactions are directly calculable from internuclear distance distributions, their measurement is of particular relevance in the structural analysis of glasses.

To the present date, however, REDOR experiments have been mainly applied to isolated pairs of spin-$^1/_2$ nuclei, in which case the theoretical description is particularly simple. In applications to inorganic glasses, however, additional complications arise because in general multiple dipolar interactions are present, and because many of the nuclear species involved have spin quantum number $>^1/_2$. While results from various research groups have demonstrated that REDOR and related techniques can provide useful qualitative information on medium range structure of glass systems,[13−18] a quantitative comprehensive discussion of a glass system has not been given to date. One important aspect and purpose of this contribution is the development of a quantitatively reliable REDOR NMR methodology for addressing this question. We will present combined ^{27}Al{^{11}B}- and ^{11}B{^{27}Al}-REDOR results on sodium aluminoborate glasses and a crystalline model compound. On the basis of detailed simulations and experimental studies as a function of composition, we will derive quantitative information about the boron−aluminum site connectivities present. In addition, analogous ^{11}B{^{23}Na} and ^{23}Na{^{11}B}-REDOR studies offer insights into the spatial distribution of the sodium cations in relation to the network, thereby providing a complementary view of glass structure from the perspective of the network modifier species.

Fundamental Principles and Methodology

REDOR NMR of Multiple-Spin Systems Involving Quadrupolar Nuclei. Figure 1 shows the REDOR pulse sequence used in the present study. This technique reintroduces the heteronuclear dipolar coupling, which is normally averaged out by MAS, into the high-resolution NMR experiment.[11,12] Basically, the magnetization associated with one spin species ("spin *S*") is observed by a rotor-synchronized Hahn-spin echo sequence, while 180° pulses are applied to the other spin species ("spin *I*") during the evolution times following the initial 90°(*S*) and the 180°(*S*) refocusing pulses. These 180° pulses reverse the sign of the *I*−*S* dipole−dipole coupling constant, thereby preventing cancellation of this interaction over the MAS rotor period. As a consequence, the *S* spin echo is attenuated. Thus,

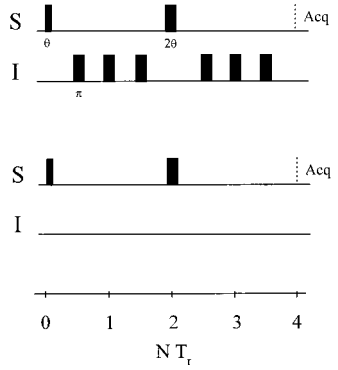

Figure 1. Basic building block (four rotor cycles) of the REDOR pulse sequence used within this study. The top part gives rise to signal intensity *S*, the bottom part to intensity S_0.

the *I*−*S* dipole−dipole coupling can be characterized by the difference signal $\Delta S = S_0 - S$ of two experiments executed in the absence (S_0) and presence (S) of the 180° pulses on the *I* spins. The magnitude of ΔS depends (a) on the size of the *I*−*S* dipole−dipole coupling constant and (b) on the length of the evolution time during which the dipolar coupling is active. This time scale is under experimental control and given by NT_r, the number of rotor cycles (N) multiplied by the period of one rotor revolution (T_r). Thus, a plot of $\Delta S/S_0$ versus NT_r provides information about the strength of the dipolar coupling. For an isolated pair of spin-$^1/_2$ nuclei it has been derived that[12]

$$\frac{\Delta S}{S_0} = 1 - \frac{1}{2\pi}\int_0^{2\pi}\int_0^{\pi/2}\cos(\Delta\Phi)\sin\beta\,d\alpha\,d\beta \qquad (1)$$

where

$$\Delta\Phi = 2\sqrt{2}NT_rD\sin 2\beta\sin\alpha \qquad (2)$$

with

$$D = \frac{\mu_o}{4\pi}\frac{\gamma_I\gamma_S\hbar}{2\pi\langle r^3\rangle} \qquad (3)$$

Here, α and β are the polar angles relating the principal axis system to the laboratory coordinate system. From a fit of the experimental REDOR curve to eq 1 the dipole−dipole coupling constant D can be extracted, which can be related via eq 3 to the vibrationally averaged value $\langle r^3\rangle$, where r is the internuclear distance. (all the other symbols in eqs 1−3 carry their usual meanings). While in principle D also includes a contribution due to the anisotropy of indirect spin−spin couplings, these can be considered negligible in the present study because direct bonds do not occur, and because the chemical bonding is fairly polar.

The situation for aluminoborate glasses is more complicated, however, because these systems do not contain isolated spin pairs but have multiple *I*−*I*, *S*−*S*, and *I*−*S* interactions. The effects of such multiple-spin interactions on REDOR dephasing have been treated theoretically for systems involving only spin-$^1/_2$ nuclei. As shown by Naito et al.,[19] the shape of the REDOR dephasing curve of a three-spin system is sensitively dependent on the geometry of the system considered. Figure 2a,b shows the results of simulations carried out in our own laboratory for distinct spin geometries, using the approach of Naito et al. Most importantly, these simulations show that for a given order of a spin system the geometry dependence of the dephasing curves is negligible in the limit of short dipolar evolution times. In

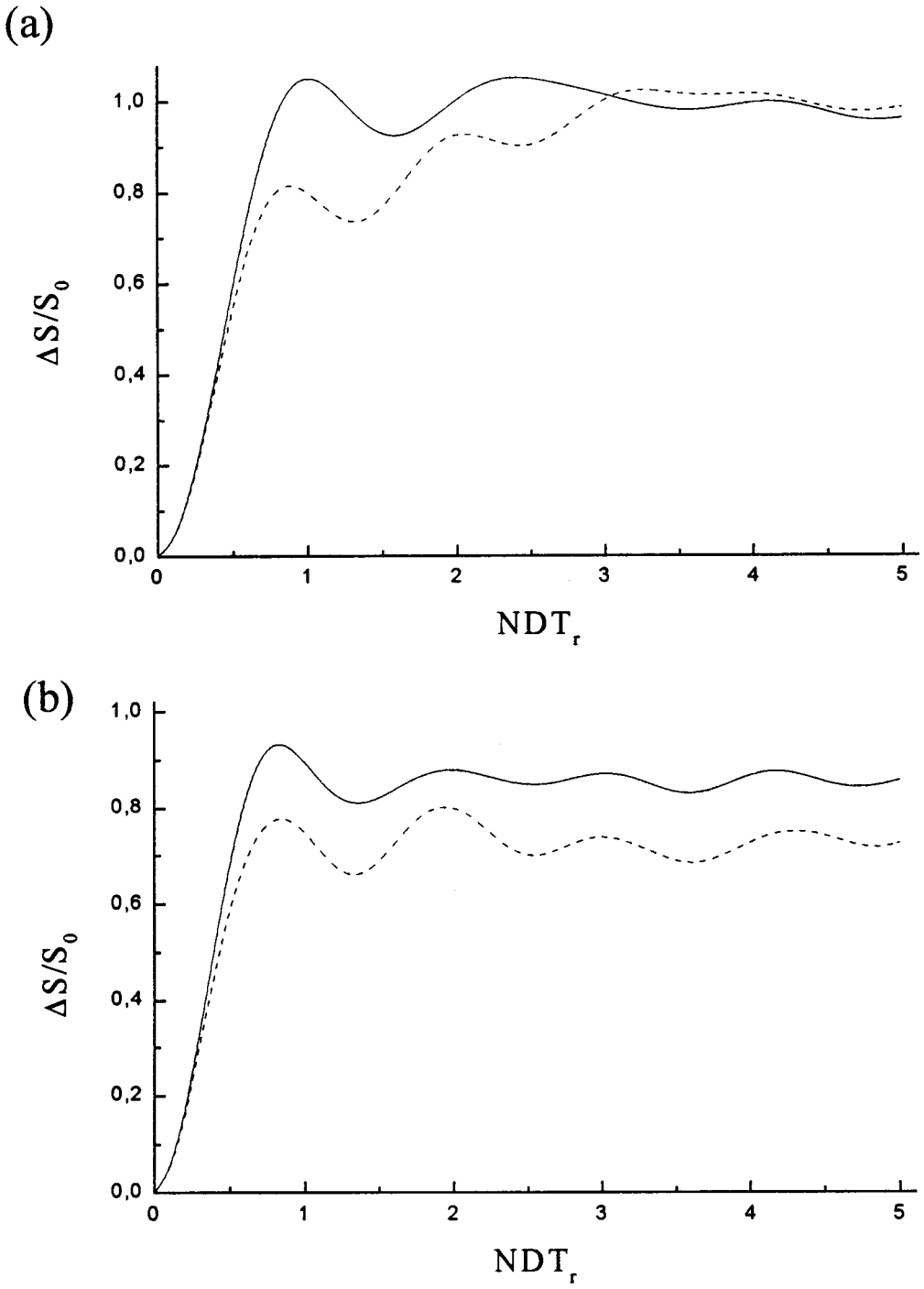

Figure 2. (a) Simulated REDOR curves of SI_3 spin systems with different geometries: comparison of trigonal planar (solid line) and trigonal pyramidal symmetry (dashed line). (b) Simulated REDOR curves of SI_4 spin systems with different geometries: comparison of tetrahedral (solid line) and square−planar symmetries (dashed line).

this limit, the REDOR dephasing curves can be approximated by a simple analytical function:[11]

$$\frac{\Delta S}{S_0} = \frac{16}{15}(NT_r)^2[D_1^2 + D_2^2 + ... + D_n^2] \quad (4)$$

where $\sum_{i=1}^{n} D_i^2$ can be related to the van Vleck heteronuclear dipolar second moment M_2^{IS},[20] resulting in the expression

$$\frac{\Delta S}{S_0} = \frac{1}{I(I+1)\pi^2}(NT_r)^2 M_2^{IS} \quad (5)$$

Here I represents the spin quantum number of the nonobserved nucleus.

$$M_2^{IS} = \frac{4}{15}\left(\frac{\mu_0}{4\pi}\right)^2 \gamma_I^2 \gamma_S^2 \hbar^2 I(I+1) \sum_I \langle r_{IS}^{-6} \rangle \quad (6)$$

In principle, eq 5 allows the dipolar coupling to be quantified in REDOR experiments on systems of unknown order and geometry. As an important feature of REDOR, site-selective heterodipolar second moments are obtained due to the high resolution afforded by MAS. Detailed simulations carried out in our laboratory[21] indicate that for isolated clusters of spin-$^1/_2$ nuclei a simple parabolic fit of experimental REDOR data to eq 5 will result in reliable second moment information, provided that the data range used for the analysis remains within the limits $0 < \Delta S/S_0 < 30\%$.

The foregoing treatment ignores the possible influence of $I-I$ dipole−dipole interactions on the shapes of the REDOR curves, a problem that has been discussed and addressed in detail by Goetz and Schaefer.[22] Yet another major complication in the application of REDOR to aluminoborate glasses arises from the fact that both ^{11}B and ^{27}Al are $I > {}^1/_2$ nuclei. Because of strong quadrupolar interactions, the various Zeeman transitions are anisotropically broadened and shifted with respect to each other. A relatively simple situation arises in the (not uncommon) case $H_Q^{(2)} \ll H_{rf} \ll H_Q^{(1)}$. In this case the first-order quadrupolar splitting is sufficiently large so that the 180° pulses affect only the spin populations contributing to the central $|^1/_2\rangle \leftrightarrow |^{-1}/_2\rangle$ transition. At the same time the linebroadening due to the second-order effects is moderately small so that the central transition is uniformly excited. Provided further that the spin−lattice relaxation times are long on the time scale of the REDOR experiment, only the I nuclei contributing to the central transition produce dephasing of S spin coherence. While this situation simplifies the problem conceptually, it is not clear how realistically it can be accomplished in practice. In fact recent simulations by Chopin et al. cast some doubts on the "central level assumption".[23] To facilitate a discussion of the present experimental results, we simply introduce a calibration factor f ($0 < f < 1$) into eq 5,

$$\frac{\Delta S}{S_0} = \frac{f}{I(I+1)\pi^2}(NT_r)^2 M_2^{IS} \qquad (7)$$

accounting for systematic errors introduced by the I−I dipolar couplings, by the quadrupolar splittings of the I nuclei, and by experimental imperfections.

The approach used in this study is to determine the calibration factor f experimentally by conducting REDOR on crystalline model compounds having similar spin dynamics as the glasses of interest. In these model compounds M_2^{IS} can be computed from the internuclear distances extracted from the known crystal structures. For $^{27}Al \leftrightarrow {}^{11}B$ REDOR experiments, the model compound $Li_6Al_2(BO_3)_4$ was chosen, where the ^{11}B and ^{27}Al quadrupolar coupling parameters and the $^{11}B-{}^{27}Al$ dipolar interaction strengths are very similar to those present in the glasses (see below). By calibrating the REDOR results on this model compound, we can quantify the $^{27}Al-{}^{11}B$ heteronuclear dipolar interaction strengths in the glasses in terms of the van Vleck dipolar second moments and relate those to the average number of $^{11}B-O-{}^{27}Al$ links present. In a similar fashion we use $^{11}B\{^{23}Na\}$- and $^{23}Na\{^{11}B\}$-REDOR results on crystalline $Na_2B_4O_7$ and $NaBO_2$ to calibrate the corresponding REDOR data for the glassy samples. By this approach we will obtain valuable information on the spatial proximity between the Na^+ ions and the boron sites.

Aside from the influence of spin dynamics it can be expected that f is also affected by experimental parameters such as the spinning frequency and the radio frequency field amplitude. Therefore, we have carefully ensured that all of the REDOR experiments are conducted under identical experimental conditions.

Experimental Section

Sample Preparation and Characterization. The sample preparation method, compositions and physical characterization data of the sodium aluminoborate glasses have been described in a previous publication (part I).[8] For the synthesis of the crystalline compound $Li_6Al_2(BO_3)_4$ the procedure from Chrysikos et al. was used.[24] Anhydrous $Na_2B_4O_7$ (Aldrich) was used without further purification. Finally, crystalline $NaBO_2$ was synthesized from $NaBO_2 \cdot 4H_2O$ (Merck) by two-step heating (110, 600 °C) until no further weight loss was observed. The X-ray diffraction patterns of these reference compounds were consistent with published literature data.[25−27]

TABLE 2: Typical Experimental Conditions for the REDOR Studies

parameter	setting
spinning frequency	6.0 kHz
recycle delay	0.2s (^{27}Al)/5s (^{11}B)/1s (^{23}Na)
90° pulse length	6.5 μs (^{27}Al)/3μs (^{11}B)
	9.5 μs (^{23}Na)/3μs (^{11}B)
number of scans	8−16 (^{11}B), 300−600 (^{27}Al,^{23}Na)

Nuclear Magnetic Resonance Studies. Standard solid-state NMR characterization of the samples has been reported previously.[8] REDOR NMR experiments were carried out on a Bruker Avance DSX-500 spectrometer equipped with a 7 mm triple resonance probe simultaneously tuned to ^{11}B (160.5 MHz) and ^{27}Al (130.3 MHz). A constant spinning frequency of 6.0 kHz was employed for all samples. To explore the effect of the experimental variables spinning frequency and rf field strength, additional experiments were conducted using a similarly configured 4 mm triple resonance probe. These REDOR studies were carried out at spinning frequencies of 6 and 12 kHz. Table 2 summarizes typical experimental conditions used. Chemical shifts are reported relative to external references of 1 M aqueous solutions of $Al(NO_3)_3$(^{27}Al), 1 M aqueous NaCl (^{23}Na), and $BF_3 \cdot OEt_2$(^{11}B),

Results and Data Analysis

^{11}B and ^{27}Al Site Speciations. Complete information on the boron and aluminum speciations in sodium aluminoborate glasses has been previously obtained in Part I of this study on the basis of field dependent MAS and triple-quantum MAS (TQMAS) NMR data.[8] The network consists of tetrahedral $BO_{4/2}^-$ units, and three types of three-coordinate boron species: trigonal $BO_{3/2}$ groups, $BO_{2/2}O^-$ species having two bridging and one nonbridging oxygen atom, and small amounts of $BO_{1/2}(O^-)_2$ units with two nonbridging and one bridging oxygen atom. (In the following the subset comprising these latter three species will be denoted as B(III) sites.) Nearly all of the aluminum atoms in sodium aluminoborate glasses are four-coordinated. These results indicate that network conversion proceeds by the reaction of the network former oxides B_2O_3 and Al_2O_3 with the O^{2-} ions introduced by the Na_2O according to the following reactions:

$$\text{(A) } 2\ AlO_{6/4} + O^{2-} \rightarrow 2\ AlO_{4/2}^-$$

$$\text{(B) } 2\ BO_{3/2} + O^{2-} \rightarrow 2\ BO_{4/2}^-$$

$$\text{(C) } 2\ BO_{3/2} + O^{2-} \rightarrow 2\ BO_{2/2}O^- (+\ BO_{1/2}(O^-)_2)$$

In the present glass system, Na^+ is the predominant counterion while eq A shows aluminum in the role of a network former species. The quantitative MAS NMR analysis of a set of 27 samples in the ternary system $Na_2O-B_2O_3-Al_2O_3$ indicates that network modification is governed by the following rules: reaction (A) always takes priority, while the extent to which reactions B and C proceed is limited by the amount of Na_2O still available after subtracting that consumed in reaction A. From this large set of samples, 10 representative compositions

TABLE 3: Glass Compositions, Percentages N_4, N_3, N_2, and N_1 of the Various Boron Sites and Fractional Contribution x_i of Each Framework Site

glass	mol %Na_2O	mol %B_2O_3	mol %Al_2O_3	N_4/%	N_3/%	$N_2(N_1)$%	x_4	x_3	$x_2(x_1)$	x_{Al}
3	25	55	20	18.8	81.2		0.138	0.595		0.266
7	30	50	20	21.8	78.2		0.156	0.559		0.286
9	30	40	30	4.2	95.8		0.024	0.547		0.429
11	35	55	10	25.4	53.5	21.1	0.215	0.453	0.178	0.154
15	35	35	30	4.2	76.8	19.0	0.023	0.414	0.102	0.462
16	38	50	12	19.8	45.8	34.4	0.160	0.369	0.277	0.194
18	40	40	20	12.0	41.4	46.6	0.08	0.276	0.311	0.333
20	40	30	30	3.2	56.4	40.3	0.016	0.282	0.202	0.5
25	50	33	17	8.8	-	78.4(12.8)	0.058	-	0.517(0.084)	0.34
27	55	30	15	5.0	-	72.3(22.8)	0.033	-	0.482(0.152)	0.333

were chosen to probe boron−aluminum connectivity by REDOR spectroscopy. In addition, sodium−boron interactions were studied on seven samples. Below we present an approximate analysis of these data and a quantitative discussion of the results obtained, as a function of composition. Table 3 summarizes the elemental compositions of these glasses as well as the fractions N_4, N_3, N_2, and N_1 of the species $BO_{4/2}^-$, $BO_{3/2}$, $BO_{2/2}O^-$, and $BO_{1/2}(O^-)_2$ as analyzed from computer fits of the ^{11}B MAS NMR spectra.[8] The values differ slightly from those given in ref 8 because we have applied the intensity correction procedure suggested by Massiot and co-workers.[29] This correction takes into account that the MAS centerband belonging to the three-coordinated boron sites does not comprise the entire intensity of the central $|^1/_2\rangle \leftrightarrow |-^1/_2\rangle$ coherence, but that some of this intensity is spread out in spinning sidebands. In contrast, the MAS centerband belonging to the $BO_{4/2}^-$ sites not only comprises the entire central coherence but also contains a small additional contribution from quadrupolar satellite transitions. Therefore, the actual N_4 values are somewhat lower than those determined from simple MAS centerband simulations. Furthermore, the ^{27}Al MAS NMR data indicate that the overwhelming fraction of aluminum is four-coordinated and hence participates in the network. While small concentrations of higher-coordinated aluminum do exist according to previous two-dimensional triple quantum MAS results,[8] these will be neglected in the analysis to follow. On the basis of a network principally composed of $BO_{4/2}^-$, $AlO_{4/2}^-$, $BO_{3/2}$, and $BO_{2/2}O^-$ units (as well as of $BO_{1/2}(O^-)_2$ in glasses 25 and 27), their respective molar fractions $x_i = n_i/\Sigma n_i$ of the network have been calculated and included in Table 3.

As discussed in part I of this study, some indirect evidence for preferential linking of these units in sodium aluminoborate glasses is based on the following observations:[8] (i) when the boron speciations of binary sodium borate glasses are compared with those of ternary sodium aluminoborate glasses with the same Na/B ratios, it is always found that in the latter the boron conversion process C is favored over process B. This finding suggests that the $AlO_{4/2}^-$ sites in the framework interact more favorably with the $BO_{2/2}O^-$ units than with the $BO_{4/2}^-$ units.

(ii) The $^{27}AlO_{4/2}$ and $^{11}BO_{4/2}$ isotropic chemical shifts in these glasses depend systematically on the sodium content. As discussed in part I, there is an excellent correlation between the δ_{iso} values of these four-coordinated species and the average connectivity of the three-coordinate boron units in the framework. This result suggests that the $BO_{4/2}^-$ and $AlO_{4/2}^-$ species interact strongly with three-coordinate boron sites in the framework. The chemical shifts of these four-coordinated species are quite sensitive to the changes in the framework, as with increasing Na_2O content of the glass the $BO_{3/2}$ units in the vicinity of $AlO_{4/2}^-$ and $BO_{4/2}^-$ groups are successively being replaced by $BO_{2/2}O^-$ groups.

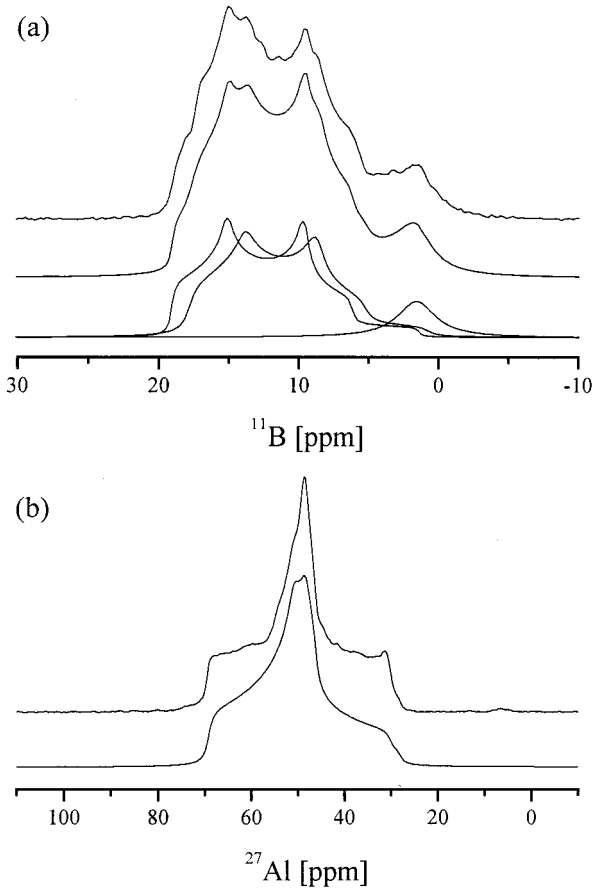

Figure 3. (a) ^{11}B-MAS spectrum of $Li_6Al_2(BO_3)_4$. The middle trace shows a simulation of the MAS line shape. The bottom trace shows the individual line shape components. (b) ^{27}Al-MAS NMR spectrum of $Li_6Al_2(BO_3)_4$. Displayed is the anisotropic F_2 projection of a triple-quantum MAS NMR spectrum. The bottom trace shows a simulation of the MAS line shape.

Since alternative interpretations of the above trends cannot be ruled out necessarily, the dipolar NMR experiments to be discussed in the following are particularly significant.

Calibration of $^{27}Al \leftrightarrow {}^{11}B$ REDOR Experiments with Crystalline $Li_6Al_2(BO_3)_4$. ^{11}B MAS and ^{27}Al MAS (anisotropic projection of the triple-quantum MAS NMR spectrum) spectra of $Li_6Al_2(BO_3)_4$ are shown in Figure 3a,b together with simulations of the powder MAS centerband line shapes. Parameters of the simulations are summarized in Table 4. From the crystal structure it is known that the boron units are of the $BO_{2/2}O^-$ type with one nonbridging oxygen.[25] The two crystallographically distinct boron sites have very similar quadrupolar coupling parameters, and the ratio of the simulated components is close to unity as predicted from the crystal

TABLE 4: Simulation Parameters of the MAS Spectra of the Crystalline Compound

compound	nucleus	δ_{iso} (ppm) (± 0.3 ppm)	C_Q (MHz) (± 0.1 MHz)	η (± 0.1)	line width (ppm) (±1 ppm)	(%)
$Li_6Al_2(BO_3)_4$	^{11}B	20.1	2.74	0.38	4	44.8
		18.6	2.68	0.40	10	47.4
		1.6	*a*		3.5	7.8[b]
	^{27}Al	69.3	6.4	0.88	8	
$NaBO_2$	^{11}B	19.1	2.52	0.8	10	96.4
		1.3	*a*		2	3.6
	^{23}Na	2.1	1.19	0.24	22	
$Na_2B_4O_7$	^{11}B	19.9	2.52	0.1	10	58.8
		2.3	*a*		2.3	41.2
	^{23}Na	−9.9	2.65	0.91	5	62
		−12.0	1.8	0.9	10	20
		−4.9	1.8	0.1	30	18

[a] Not determined. [b] Assigned to an amorphous impurity.

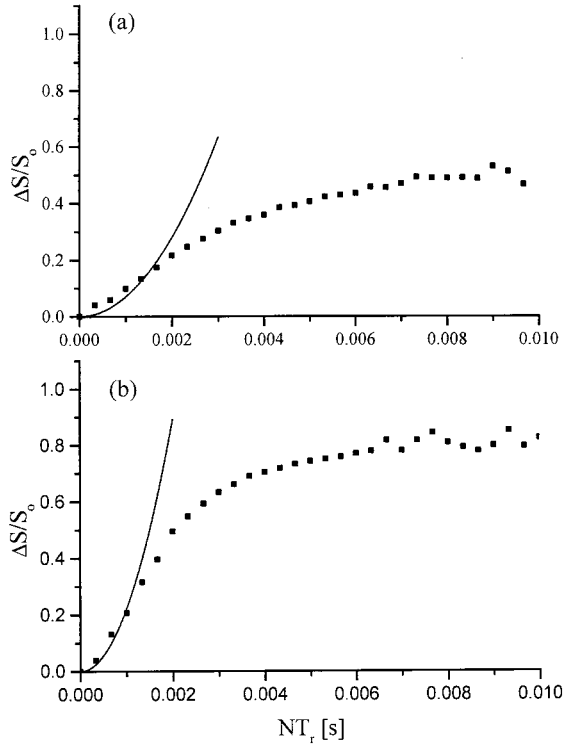

Figure 4. (a) $^{11}B\{^{27}Al\}$-REDOR curves of $Li_6Al_2(BO_3)_4$. The solid curve shows a parabolic fit to eq 5. (b) $^{27}Al\{^{11}B\}$-REDOR data points of $Li_6Al_2(BO_3)_4$. The solid curve shows a parabolic fit to eq 5.

structure. The ^{27}Al TQMAS and SATRAS experiments (data not shown) reveal a single aluminum site with spectroscopic parameters typical of four-coordinate aluminum. In the second coordination sphere each aluminum has four boron next nearest neighbors while each boron is linked via oxygen to two aluminum atoms. The average B−O−Al next nearest neighbor distance is 278 pm.[25]

The $^{27}Al\{^{11}B\}$- and $^{11}B\{^{27}Al\}$-REDOR experiments carried out on this model compound are shown in Figure 4. By fitting the initial part of each REDOR curve up to a difference signal of 20%−30% to eq 5 approximate experimental second moments can be extracted. These have to be compared with the theoretical second moments calculated via eq 6 from the crystal structure. In the $^{27}Al\{^{11}B\}$ experiment, the natural abundance of ^{11}B (80.42%) also has to be taken into account. Table 5 summarizes the experimental and calculated second moments and the resulting calibration factors determined from this comparison. The calibration factors comprise the effects of various sources of systematic error, including (a) the approximations made in the analysis acording to eq 5, (b) possible interference effects from $I-I$ dipole−dipole couplings, (c) the fact that, owing to the presence of large quadrupolar splittings only a fraction of the I nuclei are actually affected by the π pulses applied in the middle of the rotor period, and (d) experimental imperfections such as finite pulse widths and resonance offset effects.

TABLE 5: Calculated and Experimental Second Moments ($M_2/10^6$ s^{-2} ± 10%) and Calibration Factors *f* Determined from the REDOR Experiments on the Crystalline Model Compounds

	$M_{2,exp}$	$M_{2,calc}$	*f*
experiment			
$^{27}Al\{^{11}B\}$	7.68	34.9	0.22
$^{11}B\{^{27}Al\}$	4.65	50.6	0.092[a]
$^{23}Na\ \{^{11}B\}(NaBO_2)$	6.09	28.4	0.22
$^{11}BO_3\{^{23}Na\}$	9.87	35.3	0.28
$^{23}Na\ \{^{11}B\}(Na_2B_4O_7)$	6.4	31.3	0.21
$^{11}BO_3\{^{23}Na\}$	3.7	19.0	0.194
$^{11}BO_4\{^{23}Na\}$	4.5	19.0	0.24
average values			
$^{27}Al\{^{11}B\}$and $^{23}Na\{^{11}B\}$			0.22
$^{11}B\{^{23}Na\}$			0.24

[a] Obtained over the $0 \le \Delta S/S_0 \le 0.20$ REDOR data range.

Since the ^{11}B and ^{27}Al dipolar and quadrupolar coupling parameters for $Li_6Al_2(BO_3)_4$ are very similar to those measured for the glasses, and since identical experimental conditions were applied throughout all of the measurements, we assume that for a given type of REDOR experiment the calibration factor f for the glasses is the same as that for the crystalline model compound. Inspection of Figure 4 reveals that the parabolic fit is quite satisfactory in the case of the short-time analysis of the $^{27}Al\{^{11}B\}$-REDOR curve, whereas the shape of the initial $^{11}B\{^{27}Al\}$-REDOR curve reveals substantial deviations from parabolic behavior. Thus, in the latter case the second moment analysis can only be viewed as approximate. Because of these deviations, the REDOR data were analyzed over the more limited data range $0 \le \Delta S/S_0 \le 0.2$ in this case. While systematic studies revealed that the numerical value of *f* depends on the range of $\Delta S/S_0$ values included in the parabolic fit, the effect is comparable for the model compound and the glasses. Therefore, the basic conclusions remain unaffected by the particular range of $\Delta S/S_0$ chosen.

Calibration of $^{23}Na \leftrightarrow {}^{11}B$ REDOR Experiments. ^{23}Na and ^{11}B MAS NMR spectra of the two crystalline model compounds $NaBO_2$ and $Na_2B_4O_7$ are shown in Figure 5 together with the simulations. Whereas the crystal structure of $NaBO_2$ is based on $BO_{2/2}O^-$ units, that of $Na_2B_4O_7$ is composed of three distinct $BO_{4/2}^-$, four $BO_{3/2}$ units and one $BO_{2/2}O^-$ unit. In the experimental ^{11}B MAS NMR spectrum, the subspectra of the

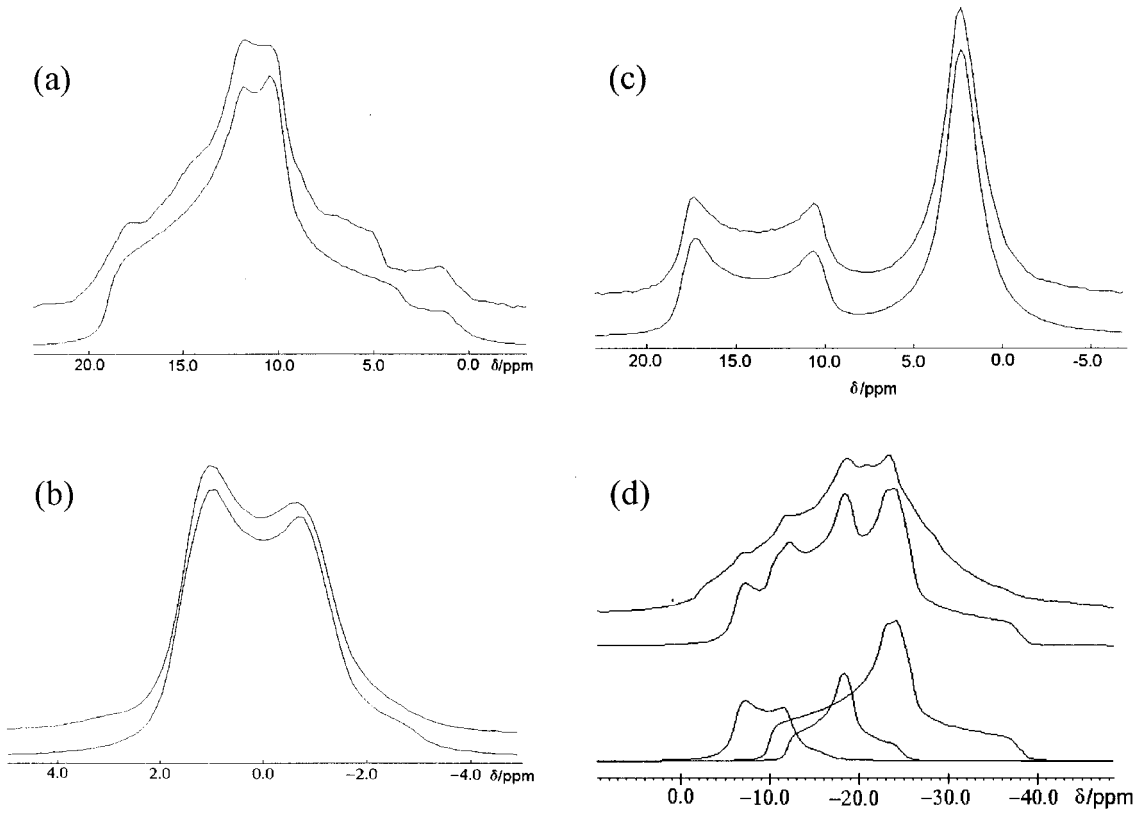

Figure 5. MAS spectra of the crystalline sodium borates together with line shape simulation; (a) ^{11}B and (b) ^{23}Na spectra of $NaBO_2$, (c) ^{11}B and (d) ^{23}Na spectra of $Na_2B_4O_7$.

latter two sites are not separable while the $BO_{4/2}^-$ units can be distinguished clearly. A satisfactory fit was obtained with two line shape components. The simulation parameters are listed in Table 4 and the percentage of $BO_{4/2}^-$ sites obtained from this fit (after the Massiot correction[29]) is close to 40% as expected. Results from ^{23}Na{^{11}B} and ^{11}B{^{23}Na}-REDOR experiments are displayed in Figure 6, together with the parabolic fits in the limit of short dipolar evolution times. The second moments and corresponding calibration factors determined as above over the data range $0 \leq \Delta S/S_0 \leq 0.3$ are given in Table 5. Note that for each type of REDOR experiment, the calibration factors are very similar for both crystalline sodium borate samples.

^{27}Al{^{11}B}-REDOR of sodium aluminoborate glasses. Figure 7 summarizes the ^{27}Al{^{11}B}-REDOR difference signals $\Delta S/S_0$ as a function of dipolar evolution time for the glassy samples studied. No significant dependence on spinning frequency and radio frequency field strength was noted, suggesting universal interpretability of these curves. Dipolar second moments, as estimated by fitting the initial decay curves ($\Delta S/S_0 < 0.30$) to eq 7 and applying the calibration factor measured for $Li_6Al_2(BO_3)_4$ are listed in Table 6.

^{11}B{^{27}Al}-REDOR of Sodium Aluminoborate Glasses. Figures 8a,b summarize the ^{11}B{^{27}Al}-REDOR results. Because of the spectroscopic resolution available in the ^{11}B MAS NMR spectra, separate REDOR curves can be obtained for the B(III) (i.e., the sum of the $BO_{3/2}$ and the $BO_{2/2}O^-$ units) and the $BO_{4/2}^-$ units, respectively. Measurements carried out under systematic variation of the experimental parameters indicate that the slopes and curvatures of these plots increase uniformly with decreasing spinning frequency and with increasing ^{27}Al rf field amplitude. As for $Li_6Al_2(BO_4)_3$, the data were analyzed over the range $0 \leq \Delta S/S_0 \leq 0.2$. For the conditions shown in Table 2, the second moments determined after correction are summarized in Table 6.

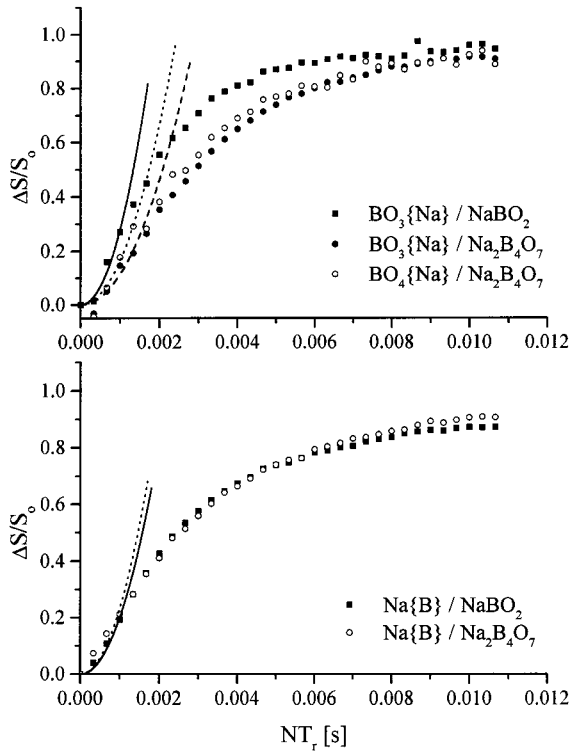

Figure 6. (a) ^{11}B{^{23}Na}-REDOR curves (at 6 kHz spinning speed) of the crystalline sodium borates; solid squares: $NaBO_2$, circles: $Na_2B_4O_7$ (solid, B(III) units; open, $BO_{4/2}^-$ units). The solid curves indicate parabolic fits to eq 5. (b) ^{23}Na{^{11}B}REDOR curves of the crystalline sodium borates: solid squares, $NaBO_2$; open circles, $Na_2B_4O_7$. The solid curves indicate parabolic fits to eq 5.

Because there is some spectral overlap of the ^{11}B signals due to three-coordinate and four-coordinate boron units on the low-

TABLE 6: Corrected Second Moments ($M_2/10^7$ s^{-2} ± 10%) of the Sodium Aluminoborate Glasses

glass	^{27}Al{^{11}B}	$^{11}BO_3${^{27}Al}^{b}	$^{11}BO_4${^{27}Al}^{b}	^{23}Na{^{11}B}	$^{11}BO_3${^{23}Na}	$^{11}BO_4${^{23}Na}
3	3.5	3.0	0.5	3.8	1.5	1.7
7	3.7	3.4	0.6	*a*	*a*	*a*
9	3.0	7.3	0.5	2.7	1.7	1.8
11	3.6	2.0	0.5	*a*	*a*	*a*
15	2.4	7.4	0.6	*a*	*a*	*a*
16	2.8	2.8	0.8	3.2	2.4	2.4
18	2.6	4.0	0.8	2.8	2.6	2.5
20	1.9	6.5	0.4	2.3	2.6	2.8
25	2.1	2.9	0.4	2.8	3.6	2.9
27	2.0	2.4	0.3	2.5	4.0	3.2

[a] Not measured. [b] REDOR data range used: $0 \leq \Delta S/S_0 \leq 0.20$.

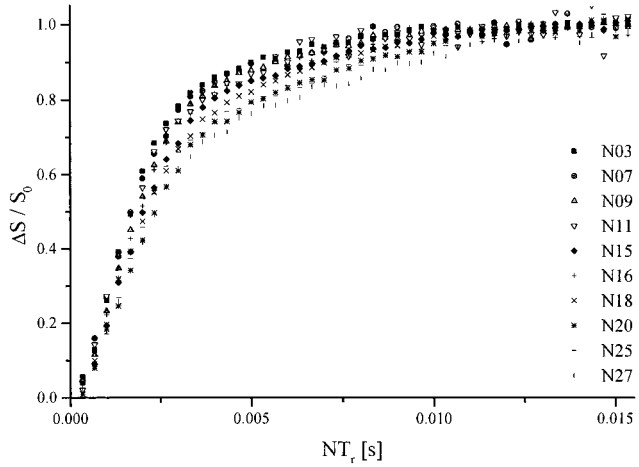

Figure 7. ^{27}Al{^{11}B}-REDOR curves of 10 sodium aluminoborate glasses.

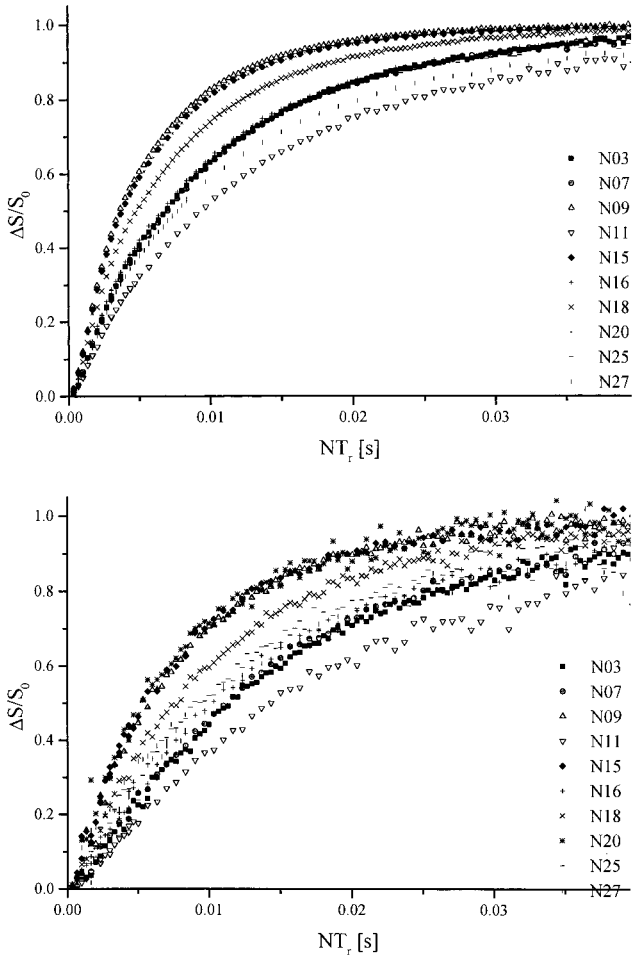

Figure 8. (a) ^{11}B{^{27}Al}-REDOR curves of the 10 glasses studied (B(III) units). (b) ^{11}B{^{27}Al}-REDOR curves of the 10 glasses studied (four-coordinated boron).

frequency side of the MAS powder pattern, the separation of the $^{11}BO_{4/2}${^{27}Al} and ^{11}B(III){^{27}Al}-REDOR curves on the basis of peak intensity measurements or integrals produces a systematic error. Especially for glasses in which the $BO_{4/2}^-$ signal is small, this error leads to an over-estimation of the dipolar coupling between $^{11}BO_{4/2}^-$ and $^{27}AlO_{4/2}^-$ groups. All of the $M_2(^{27}Al-^{11}BO_{4/2}^-)$ values listed in Table 6 have been corrected for this effect by subjecting the individual spectra comprising a set of REDOR data for selected glass samples to explicit line shape simulation.

For each single glass, the $^{27}Al-^{11}BO_{3/2}$ dipole−dipole couplings are found to be significantly stronger than the corresponding $^{27}Al-^{11}BO_{4/2}^-$ interactions. This difference is illustrated in Figure 9 for one selected glass sample.

^{23}Na{^{11}B}-REDOR and ^{11}B{^{23}Na}-REDOR of Sodium Aluminoborate Glasses. Figure 10 summarizes ^{23}Na{^{11}B}-REDOR results obtained on seven sodium aluminoborate glasses. The REDOR curves depend very little on experimental conditions and are moderately dependent on sample composition. The ^{11}B{^{23}Na}-REDOR curves are shown in Figure 11a,b. Unlike the case of the boron−aluminum interaction discussed above, the present ^{11}B{^{23}Na}-REDOR results reveal that B(III) and $BO_{4/2}^-$ units interact about equally strongly with the sodium ions. For both types of REDOR experiments, the M_2 values obtained by fitting the initial part of the REDOR curves to eq 5 followed by calibration with the crystalline model compounds are included in Table 6.

Discussion

Quantification of Network Connectivities in Sodium Aluminoborate Glasses. Figure 12 correlates the heteronuclear dipolar second moments $M_2(^{27}Al-^{11}B)$ measured by ^{27}Al{^{11}B}-REDOR with the B/Al ratio. Likewise, Figure 13 correlates $M_2(^{11}B-^{27}Al)$ values as measured from ^{11}B{^{27}Al}-REDOR, with the Al/B ratio of the glass. As indicated in these figures, the average number of B−O−Al links in these glasses can be estimated from these data, using the following procedure: In both crystalline $Li_6Al_2(BO_3)_4$ and the glassy samples, by far the dominant contribution to the strength of the $^{11}B-^{27}Al$ heteronuclear dipole−dipole interaction arises from the next-nearest neighbor coupling across a B−O−Al linkage. In $Li_6Al_2(BO_3)_4$ where each aluminum site is coordinated by four boron atoms, the heterodipolar contribution of the ^{11}B spins to the second moment of the ^{27}Al resonance is 3.49×10^7 s^{-2}, i.e., (via linear scaling) 0.87×10^7 s^{-2} per B−O−Al link present. When we compare this number with the $M_2(^{11}B-^{27}Al)$ values measured for the glasses, we can deduce approximate

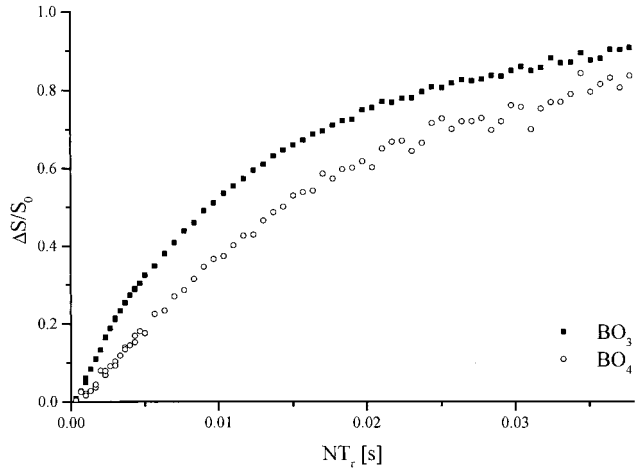

Figure 9. Comparison of REDOR curves of glass 11 for the B(III) units (solid squares) and four-coordinated boron units (open circles).

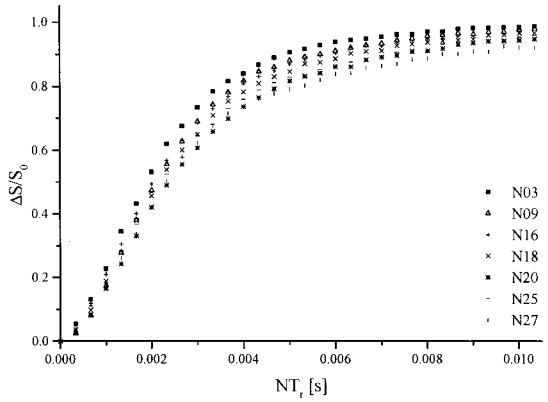

Figure 10. ^{23}Na{^{11}B}-REDOR curves of seven glasses studied.

average numbers of boron atoms in the aluminum second coordination sphere. In an analogous fashion, we obtain the average number of aluminum atoms in the second coordination sphere of the two types of distinguishable boron sites. This information is summarized in Table 7 and compared with the respective predictions made from two different bonding scenarios, described as follows.

A Statistical Connectivity Scenario. If no connectivity preferences exist among the various framework species, the concentrations of B−O−Al links are simply given by statistics. With the expression

$$Y = 4x_{Al} + 4x_{B4} + 3x_{B3} + 2x_{B2} + x_{B1} \qquad (8)$$

denoting the total sum of bonds originating from network former sites, the statistical prediction for the number of next-nearest boron neighbors per four-coordinated aluminum atom is given by

$$N_B(Al) = \left(\frac{16x_{B4} + 12x_{B3} + 8x_{B2} + 4x_{B1}}{Y}\right) \qquad (9)$$

taking into account the mole fraction and the number of bonds originating from each site. In the ^{11}B-detected REDOR experiments, we can separately estimate connectivities for four- and three-coordinate boron species. The statistical number of aluminum next nearest neighbors to a $BO_{4/2}^-$ site is given by

$$N_{Al}(B4) = \frac{16x_{Al}}{Y} \qquad (10)$$

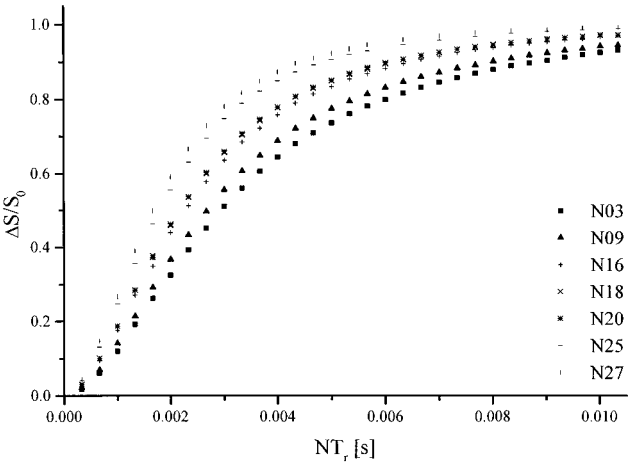

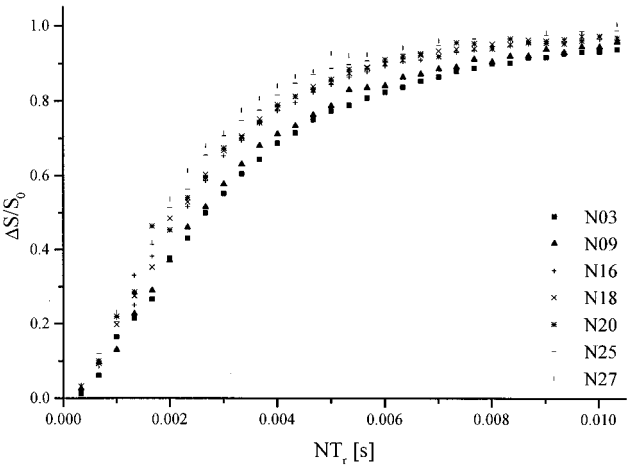

Figure 11. ^{11}B{^{23}Na}-REDOR curves of seven glasses studied: (top) B(III) units, (bottom) four-coordinated boron units.

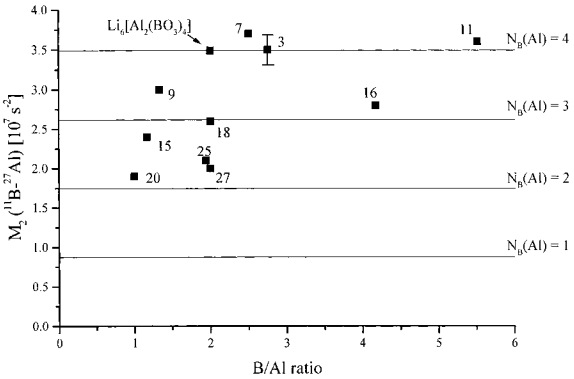

Figure 12. Correlation of the heteronuclear second moments of the ^{27}Al{^{11}B}-REDOR experiment with the B/Al ratio. Solid lines indicate the second moment values belonging to integer values of $N_B(Al)$. The vertical bar shows an estimation of the experimental error.

Since the various three-coordinated boron species are always detected jointly, the experimental REDOR data yield an average number of aluminum sites next to them. The statistical prediction can be calculated from the expression

$$N_{Al}(B3 + B2 + B1) = \frac{4x_{Al}}{Y}\frac{3x_{B3} + 2x_{B2} + x_{B1}}{x_{B3} + x_{B2} + x_{B1}} \qquad (11)$$

Table 7 compares these predictions to the experimental values. The inadequacy of the statistical connectivity scenario is particularly revealed by the large discrepancies observed for

TABLE 7: Average Number of Boron Framework Species Linked to an Aluminum Site, Average Number of Aluminum Species Linked to the Combined Subset of $BO_{3/2}$, $BO_{2/2}O^-$, and $BO_{1/2}(O^-)_2$ Sites, Average Number of Aluminum Linked to Four-Coordinate Boron Sites, and Al−O−B Connectivity Index Deduced from Each REDOR Experiment: The Experimental Data Are Compared with the Predictions Made for the Statistical and the Preferential Connectivity Scenarios

	N_B(Al)			N_{A1}(B3+B2+B1)			N_{Al}(B4)			Y(B−O−Al)			
										experimental		N(B−O−Al)	
glass	exptl	statistical	preferential	exptl	statistical	preferential	exptl	statistical	preferential	$^{11}B\{^{27}Al\}$	$^{27}Al\{^{11}B\}$	statistical	ordered
3	4.0	2.73	4.00	0.8	0.95	1.82	0.2	1.27	0	0.72	1.08	0.74	1.08
7	4.2	2.66	3.53	0.8	1.01	1.81	0.3	1.34	0	0.80	1.23	0.77	1.01
9	3.4	2.02	3.62	2.2	1.49	2.84	0.2	1.98	0	1.58	1.48	0.87	1.55
11	4.1	3.25	4.00	0.5	0.51	0.95	0.2	0.75	0	0.54	0.62	0.49	0.60
15	2.7	1.83	2.95	2.2	1.52	2.64	0.2	2.17	0	1.52	1.27	0.84	1.36
16	3.2	3.01	3.92	1.0	0.64	1.18	0.3	0.98	0	0.77	0.61	0.57	0.76
18	3.0	2.30	3.42	1.6	1.05	1.94	0.3	1.70	0	0.95	0.98	0.76	1.14
20	2.2	1.58	2.35	2.1	1.56	2.43	0.2	2.42	0	1.23	1.09	0.79	1.18
25	2.4	2.03	2.70	1.1	0.91	1.53	0.2	1.97	0	0.71	0.80	0.67	0.92
27	2.3	1.95	3.00	0.8	0.90	1.57	0.1	2.05	0	0.61	0.76	0.64	1.00

the $^{11}BO_{4/2}^-$ sites. Simple statistics would predict a four-coordinate boron species to engage in a larger number of B−O−Al links on average than any of the three-, two-, or one-coordinate boron species. Thus, in a statistical scenario the $BO_{4/2}^-$ units should exhibit the stronger coupling to ^{27}Al, opposite to the experimental observation. Our experimental results are thus in complete disagreement with the statistical model.

A Scenario of Preferential Connectivities. This model is based on preferential linking between the three-coordinate boron sites $BO_{3/2}$, $BO_{2/2}O^-$, and $BO_{1/2}(O^-)_2$ with the tetrahedral $AlO_{4/2}^-$ and $BO_{4/2}^-$ sites and on the avoidance of intertetrahedral links which are considered energetically unfavorable on the basis of the bond valence arguments discussed above (see Introduction). Thus, in glasses having sufficient concentrations of B(III) units, each aluminum site will have four boron next nearest neighbors. In those glasses, where the number of B(III) units is not sufficiently large, aluminum will be bonded to as many B(III) units as possible, and some residual $AlO_{4/2}-AlO_{4/2}$ and/or $AlO_{4/2}-BO_{4/2}$ links will be present. In calculating the number of possible boron links to aluminum we have to consider further that the $BO_{4/2}^-$ units, which are also present, occupy additional linkage sites at the B(III) species. Assuming that those $BO_{4/2}^-$ units are exclusively linked to three-coordinate boron, the number of boron units surrounding each aluminum atom can be predicted

$$N_B(\mathrm{Al}) = \frac{3x_{B3} + 2x_{B2} + x_{B1} - 4x_{B4}}{x_{A1}} \qquad (12)$$

For the boron observed case, this scenario implies the absence of any aluminum in the coordination sphere of the $BO_{4/2}^-$ units, while the number of $AlO_{4/2}^-$ sites surrounding a B(III) site is maximized. At low Al contents, the average number of aluminum atoms per three-coordinated boron atom is controlled by the mole fraction of aluminum in the network and calculated from

$$N_{Al}(\mathrm{B}) = \frac{4x_{A1}}{x_{B3} + x_{B2} + x_{B1}} \qquad (13)$$

At high Al contents, the number of available coordination sites at B(III) limits the extent of B−O−Al bond formation. Assuming again that $BO_{4/2}^-$ units occupy available B(III) sites only, the average number of aluminum sites per B(III) unit is given by

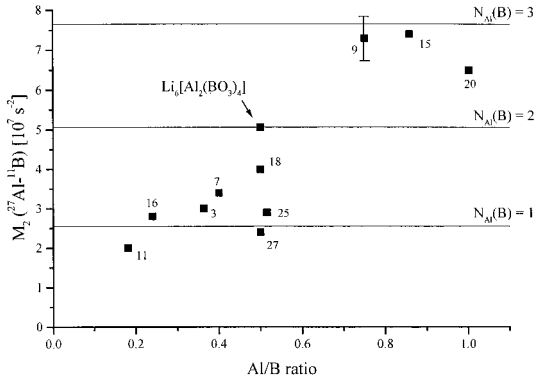

Figure 13. Correlation of the heteronuclear second moments from the $^{11}B\{^{27}Al\}$-REDOR experiment (B(III) groups only) with the Al/B ratio. Solid lines indicate the second moment values belonging to integer values of N_{Al}(B). The vertical bar shows an estimation of the experimental error.

$$N_{Al}(\mathrm{B}) = \frac{3x_{B3} + 2x_{B2} + x_{B1} - 4x_{B4}}{x_{B3} + x_{B2} + x_{B1}} \qquad (14)$$

The appropriate number of N_{Al}(B) is then always the smaller of the two numbers calculated from eqs 13 or 14.

Comparison of Both Scenarios with Experimental Data. Table 7 compares the theoretical predictions of both scenarios with the experimental data. Note that in both types of REDOR experiments the results strongly suggest a high degree of preferential linking in these glasses. This becomes particularly clear in those parts of the table where the next-nearest neighbor environments for the tetrahedral $BO_{4/2}^-$ units and the $AlO_{4/2}^-$ units are shown. In the case of the trigonal boron species five of the 10 glasses studied also show results more consistent with the preferential connectivity scenario, whereas for the other five glasses the results suggest a more randomized environment. As exemplified by the behavior of the glasses 25 and 27, the presence of high sodium contents appears to result in a tendency for a more statistical distribution.

Note that the average number of B−O−Al links determined by the $^{27}Al\{^{11}B\}$-REDOR experiments must be in reasonable agreement with the corresponding value obtained from the independent $^{11}B\{^{27}Al\}$-REDOR experiments. This internal consistency criterion is summarized by the equation

$$Y_{B-O-Al} = x_{Al} \cdot N_B(\mathrm{Al}) = (x_{B3} + x_{B2} + x_{B1})N_{Al}(\mathrm{B(III)}) + x_{B4}N_{Al}(BO_{4/2}) \qquad (15)$$

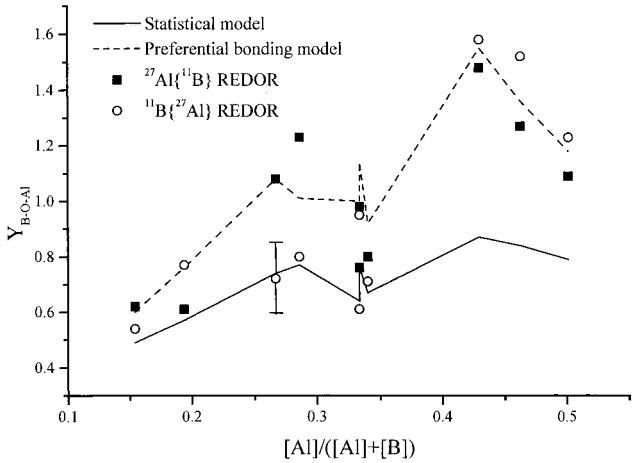

Figure 14. Index Y_{Al-O-B} denoting the total number of Al−O−B linkages in sodium aluminoborate glasses plotted as a function of the compositional parameter [Al]/([Al]+[B]). Circles: experimental results from ^{27}Al{^{11}B}-REDOR. Squares: experimental results extracted from ^{11}B{^{27}Al}-REDOR (B(III) groups only). The vertical bar shows an estimation of the experimental error. Solid line: prediction from the statistical connectivity scenario. Dashed line: prediction from the preferential connectivity model.

Here, the bond index Y_{B-O-Al} can be calculated independently from both types of REDOR experiments. Table 7 illustrates acceptable consistency for seven out of 10 glasses. For samples 3, 7, and 27, however, the estimates from ^{27}Al{^{11}B}-REDOR and from ^{11}B{^{27}Al}-REDOR differ widely from each other, the number deduced from the ^{11}B-observed experiments consistently being the lower one. At present, we are not able to resolve this discrepancy although it is worth noting that it concerns all of those glasses with relatively low Al contents and large fractions of four-coordinate boron species. Overall we consider the results from ^{27}Al{^{11}B}-REDOR more reliable because they were found to be much less susceptible to variations in experimental conditions (spinning speeds, radio frequency power) than the ^{11}B{^{27}Al}-REDOR data. Also effects of fast spin−lattice relaxation must be considered. In contrast with the fairly long (1s) T_1 values of ^{11}B, the spin−lattice relaxation times of ^{27}Al are on the order of 10 ms. Therefore, ^{27}Al spin−lattice relaxation occurring during the rotor cycle may not be negligible, producing interference with the effect of the ^{27}Al π pulses on the ^{11}B spin echo intensities. Figure 14 compares the bond index Y_{B-O-Al} as extracted from both experiments with the predictions made by the two scenarios. This plot strongly supports a high degree of bonding regularity in sodium aluminoborate glasses, particularly in glasses with high aluminum contents and low $BO_{4/2}^-$ concentrations. In contrast, the network of glasses with low aluminum contents and high $BO_{4/2}^-$ concentrations appears to be organized in a more random fashion. This result suggests that $BO_{4/2}^-$ units tend to repel each other more strongly than $AlO_{4/2}^-$ groups, so that in glasses with high $BO_{4/2}^-$ contents, any bonding preferences of the $AlO_{4/2}^-$ sites have only second priority. To confirm this possible explanation, additional studies on more glass compositions would be necessary.

Interactions of Sodium with Boron in the Network. Figure 15 shows the second moments extracted from the ^{23}Na{^{11}B}-REDOR experiments using an analogous calibration procedure as described above. The values show a good correlation with the B/Na ratio. Since the oxygen atoms that comprise the coordination sphere of the sodium ions are either bonded to boron or to aluminum atoms in the framework, the number of boron atoms in the second coordination sphere of ^{23}Na (and hence the magnitude of the corresponding M_2(^{23}Na{^{11}B}) values) is expected to scale with the fractional contribution of all boron sites to the network, provided chemical segregation effects are absent. This prediction is borne out well by the experimental data. Furthermore, Figure 16 shows a strong correlation of the M_2(^{11}B{^{23}Na}) second moments with the Na/B ratio in the glass, which is again consistent with a more or less homogeneous cation distribution. Contrary to the aluminum network coformer, the sodium network modifier species interact equally strongly with the $BO_{4/2}^-$ groups as with the various types of the B(III) species. Closer inspection (at different values of the evolution time) of the REDOR curves reveals further that the neutral $BO_{3/2}$ groups and the anionic $BO_{2/2}O^-$ groups interact equally strongly with the sodium cations. All of these results are consistent with a close-to-homogeneous distribution of the sodium cations throughout the network, where a sizable fraction of the oxygen atoms in the first coordination sphere are bridging oxygen species. Any hypothetical scenarios involving clustering of sodium cations around the anionic $AlO_{4/2}^-$, $BO_{4/2}^-$, and $BO_{2/2}O^-$ species are ruled out by these experiments.

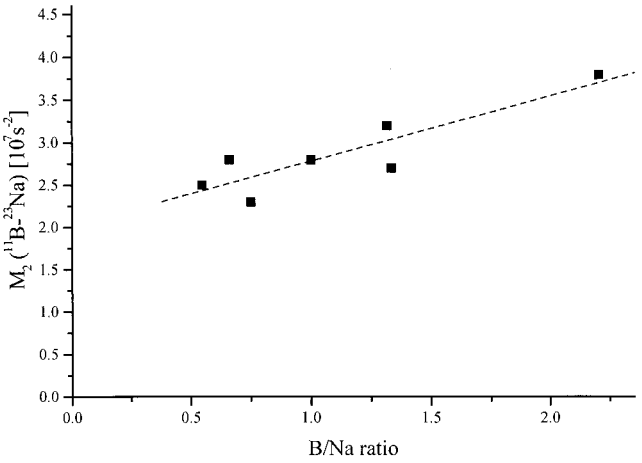

Figure 15. Correlation of the heteronuclear second moments of the ^{23}Na{^{11}B}-REDOR experiment with the B/Na ratio.

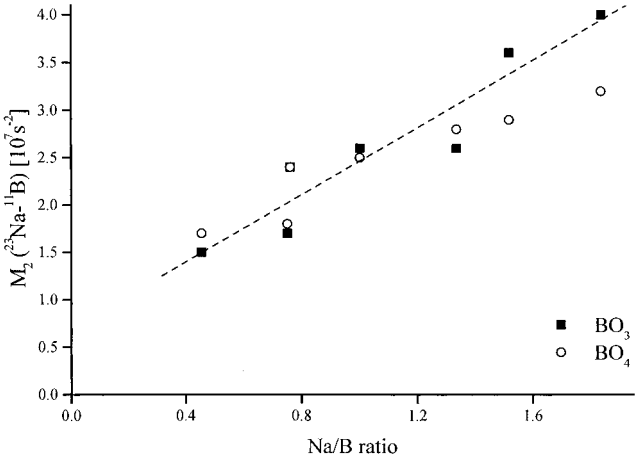

Figure 16. Correlation of the heteronuclear second moments from the ^{11}B{^{23}Na}-REDOR experiment with the Na/B ratio.

Conclusions

Overall, there is now a considerable body of experimental data, from simple one-pulse MAS NMR spectra to advanced double-resonance experiments, supporting a high degree of preferential bonding in sodium aluminoborate glasses. Consistent

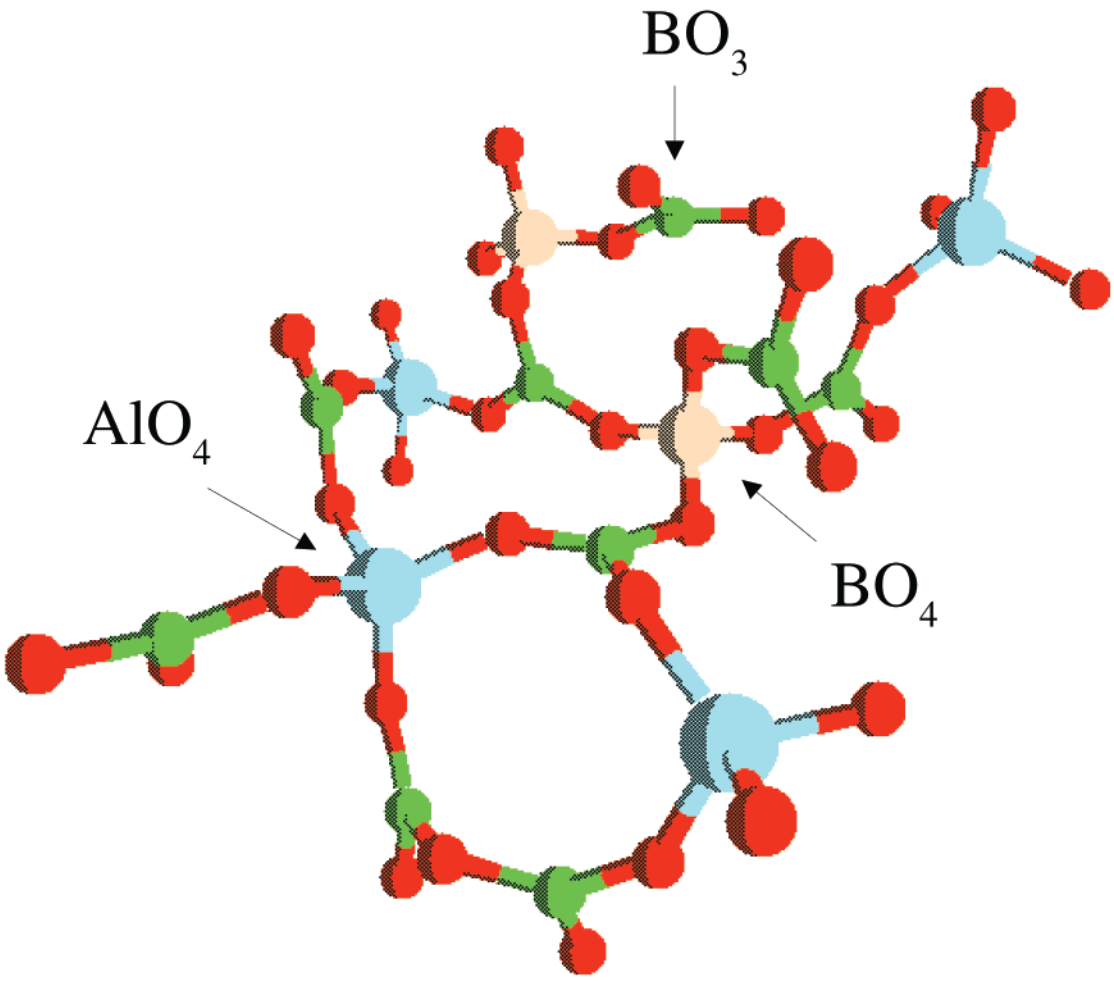

Figure 17. Pictorial description of the preferred connectivities in sodium aluminoborate glasses.

with bond valence predictions, the anionic four-coordinated units, $AlO_{4/2}^-$ and $BO_{4/2}^-$, tend to avoid bonding to each other directly and form preferential links to three-coordinated boron units in the network. The near-homogeneous distribution of charge over the network is mirrored by a homogeneous distribution of sodium ions, suggested from complementary $^{11}B \leftrightarrow {}^{23}Na$ REDOR experiments. Figure 17 gives a pictorial impression of the extended networks formed in this glass system.

The bond valence effect dominating the network of sodium aluminoborate glasses is analogous to the situation encountered in the tetrahedral framework structure of many zeolites, where the aluminum avoidance principle is known as the Löwenstein rule.[30] Compared to zeolites, however, the rule appears to be less rigorously followed in glasses, especially, when the sodium concentration is large or if sodium cations are being replaced by cations of higher ionic field strengths such as Mg^{2+} and Ca^{2+}.[10] Thus, $^{11}B \leftrightarrow {}^{27}Al$ REDOR data recently published by us on calcium and magnesium aluminoborate glasses indicate that B(III) and B(4) units interact equally strongly with aluminum suggesting a significantly lower tendency of ordering in the network.[14] To examine the validity of such simple ordering principles, we are currently extending our NMR studies of preferred network connectivities to other systems based on two or more network former components.

Acknowledgment. We thank Mrs. Heike Kamps for the preparation and the thermoanalytical characterization of the glass samples. Valuable discussions with Dr. Leo van Wüllen (WWU Münster) are also gratefully acknowledged. Financial support of this research by the Wissenschaftsministerium Nordrhein-Westfalen and by the Fonds der chemischen Industrie is gratefully appreciated. Jerry C. C. Chan thanks the Alexander-von-Humboldt Foundation for a personal stipend.

References and Notes

(1) Eckert, H. *Prog. NMR Spectrosc.* **1992**, *24*, 159.
(2) Eckert, H. *NMR: Basic Princ. Prog.* **1994**, *33*, 131.
(3) Bray, P. J.; Gravina, S. J.; Hintenlang, D. H.; Mulkern, R. V. *Magn. Reson. Rev.* **1988**, *13*, 263.
(4) Elliott, S. R. *Nature* **1991**, *354*, 445.
(5) Gresch, R.; Müller-Warmuth, W.; Dutz, H. J. *Noncryst. Solids* **1976**, *21*, 31.
(6) Zhong, J.; Bray, P. J. *J. Noncryst. Solids* **1986**, *84*, 17.
(7) Hähnert, M.; Hallas, E. *Rev. Chim. Mineral.* **1987**, *24*, 221.
(8) Züchner, L.; Chan, J. C. C.; Müller-Warmuth, W.; Eckert, H. *J. Phys. Chem. B* **1998**, *102*, 4495.
(9) Bunker, B. C.; Kirkpatrick, R. J.; Brow, R. K.; Turner, G. L.; Nelson, C. *J. Am. Ceram. Soc.* **1991**, *74*, 1430.
(10) Bunker, B. C.; Kirkpatrick, R. J.; Brow, R. K. *J. Am. Ceram. Soc.* **1991**, *74*, 1425.
(11) Gullion, T.; Schaefer, J. *J. Magn. Reson.* **1989**, *81*, 196.
(12) Pan, Y.; Gullion, T.; Schaefer, J. *J. Magn. Reson.* **1990**, *90*, 330.
(13) Van Wüllen, L.; Züchner, L.; Müller-Warmuth, W.; Eckert, H. *Solid State Nucl. Magn. Reson.* **1996**, *6*, 53.
(14) Chan, J. C. C.; Bertmer, M.; Eckert, H. *J. Am. Chem. Soc.* **1999**, *121*, 5238.
(15) DePaul, S. M.; Ernst, M. Shore, J. A.; Stebbins, J. F.; Pines, A. *J. Phys. Chem.* B **1997**, *101*, 3240.
(16) Van Wüllen, L.; Züchner, L.; Bertmer, M.; Eckert, H. *Ber. Bunsen-Ges. Phys. Chem.* **1996**, *100*, 1539.
(17) Rong, C.; Wong-Moon, K. C.; KLi, H.; Hrma, H.; Cho, H. *J. Noncryst. Solids* **1998**, *223*, 32.
(18) Wenslow, T.; Müller, K. T. *J. Noncryst. Solids* **1998**, *231*, 78.

(19) Naito, A.; Nishimura, K.; Tuzi, S.; Saito, H. *Chem. Phys. Lett.* **1994**, *229*, 506.
(20) Van Vleck, J. H. *Phys. Rev*. **1948**, *54*, 1168.
(21) Bertmer, M.; Eckert, H. *Solid State Nucl. Magn. Reson.* **1999**, *16*, 139.
(22) Goetz, J. M.; Schaefer, J. *J. Magn. Reson.* **1997**, *127*, 147.
(23) Chopin, L.; Vega, S.; Gullion, T. *J. Am. Chem. Soc.* **1998**, *120*, 4406.
(24) Chryssikos, G. D.; Bitsis, M. S.; Kapoutsis, J. A.; Kamitsos, E. I. *J. Noncryst. Solids* **1997**, *217*, 278.
(25) Abdullaev, G. K.; Mamedov, K. S. *Sov. Phys. Crystallogr*. **1982**, *27*, 229.
(26) Hyman, A.; Perloff, A.; Mauer, F.; Block, S. *Acta Crystallogr*. **1967**, *22*, 815.
(27) Krogh-Moe, J. *Acta Crystallogr. B* **1974**, *30*, 578.
(28) Amoureux, J. P.; Fernandez, C.; Steuernagel, S. *J. Magn. Reson*. **1996**, *A123*, 116.
(29) Massiot, D.; Bessada, C.; Coutures, J. P.; Taulelle, F. *J. Magn. Reson*. **1990**, *90*, 231.
(30) Loewenstein, W. *Am. Mineral.* **1954**, *39*, 92.